RSC Advances

PAPER

View Article Online
View Journal | View Issue

Cite this: *RSC Adv.*, 2017, **7**, 31164

Structure–property relationship study of Nafion XL membrane for high-rate, long-lifespan, and all-climate vanadium flow batteries†

Lihong Yu,*[a] Feng Lin,[a] Ling Xu[a] and Jingyu Xi*[b]

Vanadium flow batteries (VFB) have become one of the most promising large-scale energy storage technologies owing to their overwhelming advantage in lifespan and power. Development of highly efficient, durable and low-cost ion exchange membranes is essential to the practical application of VFB. In this work, we report an ultra-thin sandwich structure membrane (Nafion XL), as a promising alternative to the widely used Nafion 212 and 115 membranes. By combination of the mechanical reinforcement though the microporous PTFE middle layer (~10 μm) and fast proton transport through the two dense Nafion outer layers (~10 μm), the Nafion XL membrane shows lower area resistance and slower vanadium ion crossover than the Nafion 212 and 115 membranes. As a result, the Nafion XL membrane-based VFB single cell demonstrates excellent rate capability (40–400 mA cm^{-2}), superior long-term cycling stability (2200 cycles@120/200 mA cm^{-2}) and wide temperature adaptability (−20 to 50 °C). The results reported herein are beneficial for the development of high-rate, long-lifespan, and all-climate VFB for sustainable energy storage.

Received 3rd May 2017
Accepted 13th June 2017

DOI: 10.1039/c7ra04996j

rsc.li/rsc-advances

1. Introduction

Vanadium flow batteries (VFB) have become one of the fastest growing and most promising options in the large-scale and highly efficient energy storage technology due to their long cycle life, easily implemented large-scale, flexible operation, and friendly environmental impact.[1–4] The VFB system utilizes the VO^{2+}/VO_2^+ redox couple as the positive electrolyte, the V^{2+}/V^{3+} redox couple as the negative electrolyte, an ion-exchange membrane (IEM) as the separator, and graphite (carbon) felt as the electrode.[5,6]

IEM is the core material of a VFB which defines the manufacturing costs, energy efficiency, and cycle stability of the VFB.[7–9] In order to meet the design life (typically 10–20 years) of VFB, an ideal IEM for VFB should own excellent proton selectivity (*i.e.* high proton conductivity and low vanadium ion permeability), outstanding chemical stability and good mechanical strength.[5,7] Up to date, the perfluorosulfonic-acid (PFSA) based Nafion series membranes[10,11] (*e.g.* Nafion 212, Nafion 115 *etc.*) have been widely used as the benchmark in VFB because of their good transport properties and remarkable chemical/mechanical stability.[12–16] However, fast crossover of vanadium ions[7,15] and the high-cost[17,18] limit its practical application in VFB. Although great achievements have been made in search of high selectivity and low-cost hydrocarbon-based IEMs for VFB application,[19–24] these nonfluoride IEMs display poor cycling stability because of the degradation by the vanadium electrolyte (*i.e.* poor chemical stability)[25–27] and/or the damages by the uneven pressure from sealing gasket (*i.e.* poor mechanical stability)[28–30] during VFB operation. Therefore, the revival of Nafion membrane for highly efficient and long life-span VFB is still an important direction. Rational selecting and using Nafion membranes may be two effective means to improve the performance and decrease the cost of VFB.[15,16,31] In previous work, we have demonstrated that a rational use of Nafion membrane (*i.e.* reasonable thickness[15] and proper pretreatment[31]) can achieve superior VFB performance (*e.g.* high coulombic and energy efficiencies, excellent rate capability, outstanding cycling stability *etc.*), because of the well tradeoff between permselectivity and intrinsic resistance[32] of Nafion membrane.

Nafion XL,[33–35] as a novel sandwich membrane designed by DuPont with better chemical/mechanical durability in proton exchange membrane fuel cells (PEMFC) application, is consisted of a microporous PTFE-rich support layer (~10 μm) impregnated on both sides with dense Nafion layer (~10 μm).[35] Thanks to the special sandwich structure, Nafion XL membranes show superior durability compared to their unreinforced analogue (Nafion).[36] It is expected that this ultra-thin (~30 μm) triple-layered structure can combine the advantages of microporous PTFE (effective mechanical reinforcement) and

[a]*School of Applied Chemistry and Biological Technology, Shenzhen Polytechnic, Shenzhen 518055, China. E-mail: yulihong@szpt.edu.cn*

[b]*Institute of Green Chemistry and Energy, Graduate School at Shenzhen, Tsinghua University, Shenzhen 518055, China. E-mail: xijy@tsinghua.edu.cn*

† Electronic supplementary information (ESI) available. See DOI: 10.1039/c7ra04996j

dense Nafion membrane (fast proton transport), offering excellent performances in VFB. This work aims to study the structure–property relationship of Nafion XL membrane towards VFB application, including area resistance, vanadium ion permeability, rate capability (40–400 mA cm^{-2}) and cycling stability (>2000 cycles) as well as wide temperature (−20 to 50 °C) performances. The benchmark Nafion 115 and Nafion 212 membranes are also evaluated for comparison. The results reported herein are beneficial for the development of high-rate, long-lifespan, and all-climate VFB for sustainable energy storage.

2. Experimental

2.1. Materials

The Nafion XL-100, Nafion 212 and Nafion 115 membranes were purchased from DuPont, and denoted as XL, 212 and 115, respectively. The 212 and 115 membranes were merged in deionized water for 24 h before use.[30,31] The XL membrane was used directly, since it is easy to curl in the water, as shown in Fig. S1.† Polyacrylonitrile (PAN) based graphite felt (GF) with 5 mm of thickness was purchased from Gansu Haoshi Carbon Fiber Co., Ltd. Other chemicals were of analytical grade and used without further purification.

2.2. Characterization

The physicochemical properties including swelling ratio[31] and VO^{2+} permeability[37] were measured as reported previously. Area resistance (AR) of the membranes was obtained by measuring the bulk (internal) resistance (R_b) of a VFB single cell (Fig. S2†) with membrane (R_1) and without membrane (R_2) by electrochemical impedance spectroscopy (EIS) on a PARSTAT 2273 electrochemical workstation.[16] The test frequencies were controlled from 100 kHz to 10 mHz with an amplitude voltage of 10 mV. AR of the membrane was calculated by the equation: $AR = (R_1 - R_2) \times S$. The effective area S is 25 cm^2.

The cross-section of the membranes was observed by scanning electron microscopy (SEM, ZEISS SUPRA® 55) and energy-dispersive X-ray spectroscopy (EDX). The samples were prepared by fracturing the membrane in liquid nitrogen. All the samples were coated with Pt before morphology observation. Mechanical property of the membranes (1 × 6 cm) was conducted on a CMT6104 (MTS-SANS) universal test machine with a tensile speed of 10 mm min^{-1}.

2.3. Single cell evaluation

The configuration of a VFB single cell is the same as in our previous work.[38,39] The photograph and detail parameters of the VFBs are listed in Table 1. Both electrolyte tanks were purged with nitrogen gas for 10 min and then sealed prior to the single cell tests. The charge–discharge of the cell was controlled by a Neware CT-3008-5V10A battery testing system. The effective area of membrane and electrode is 25 cm^2 (5 cm × 5 cm). Rate performance was evaluated under the current density range from 80 mA cm^{-2} to 400 mA cm^{-2}. Cycling performance was conducted under the current density of 120 mA cm^{-2} and 200 mA cm^{-2}. All-climate test was performed using a thermostat (Hongzhan PU-80) to control the temperature range from −20 to 50 °C with the deviation of ±0.5 °C.

3. Results and discussion

3.1. Morphology and transport properties

The morphology of the XL membrane is characterized by SEM, as shown in Fig. 1 and the elements distribution is also analyzed by EDX as well. The cross-section of the XL membrane (Fig. 1b) clearly reveals a sandwich structure, composited of a microporous PTFE-rich reinforce layer (around 10 μm) and two thin dense Nafion layers (around 10 μm) on both sides.[33] Therefore, the XL membrane shows translucent gray (Fig. 1a) and is prone to curl over when immersed in water (Fig. S1b†). The novel sandwich structure is also confirmed by the F and S elements mapping images (Fig. 1c), in which the F element (corresponding to the perfluorinated skeleton in both PTFE and Nafion) is more dense in the middle layer, while S element (corresponding to the $-SO_3^-$ groups in Nafion ionomer) is mainly distributed in the two out layers. In addition, Si element (corresponding to the silica additive in Nafion ionomer)[33] is mainly locating in the two Nafion layers. This is consistent with the elements configuration of the composite materials.[33–35] The Al and Pt signal in the EDX spectra can be attributed to the Al sample stage and Pt coating, respectively. Although the thickness of the XL membrane is only about 30 μm, the sandwich structure may provide an excellent mechanical strength (enabled by the middle PTFE-rich microporous layer) and fast

Table 1 Parameters of VFB single cells

Photograph	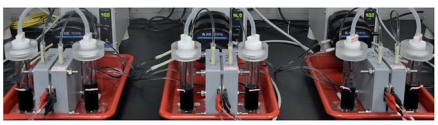		
Membrane	XL	212	115
Electrode	Graphite felt, 5 × 5 × 0.5 cm; thermal activated at 420 °C for 10 h (ref. 40)		
Electrolyte	1.5 M $V^{3.5+}$ (VO^{2+}/V^{3+} = 1/1) in 2 M free H_2SO_4,[41] 50 mL (theoretical capacity of 2.01 A h); flow rate: 60 mL min^{-1}		
Cut-off voltage	Charge: 1.65 V; discharge: 0.8 V		

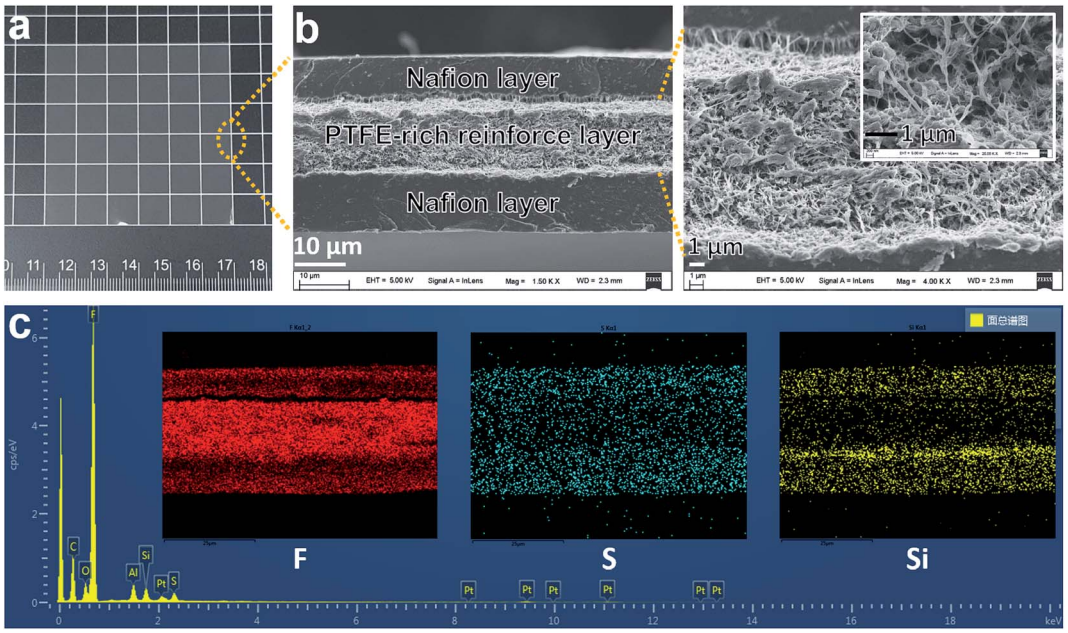

Fig. 1 Morphology of the Nafion XL membrane: (a) photograph, (b) cross-section SEM images with different magnification, and (c) EDX spectra and element mapping images.

proton conductivity (enabled by the outer Nafion dense layer) for practical VFB application. Moreover, the ultra-thin structure is also beneficial to reduce the cost of membrane.[17]

Mechanical properties are one of the most important indicators of IEMs for VFB. Stress–strain curves of various Nafion membranes are compared in Fig. 2a. The 212 and 115 membranes keep transparent before (inset of Fig. 2a) and after (Fig. 2b) fracture, while the XL membrane turns nontransparent from sub-transparent during the stretching process due to the deformation of the middle microporous PTFE layer. The obtained mechanical properties are compared in Fig. 2c. It is worth noting that the XL membrane stands the highest breaking strength and elastic modulus among the three membranes, which verifies the excellent mechanical properties of the XL membrane. The superior mechanical stability of the XL membrane can be attributed to its novel sandwich structure (Fig. 1b), in which the middle porous PTFE-rich layer serves as a reinforce scaffold.

Table 2 summarizes the physicochemical and transport properties of various Nafion membranes. All Nafion membranes would unavoidably encounter the thickness (through-plane) and area (in-plane) enlargement in the water because of the swelling of the ionic micelle nanostructure,[10,11] which will in return affect their nanostructure and transport properties (*i.e.* the preferred proton transfer and the undesired vanadium ion crossover in VFB system).[7] The through-plane swelling ratio of the XL membrane is much bigger than those of 212 and 115 membranes (33.3% *vs.* 17.3% and 20.0%),

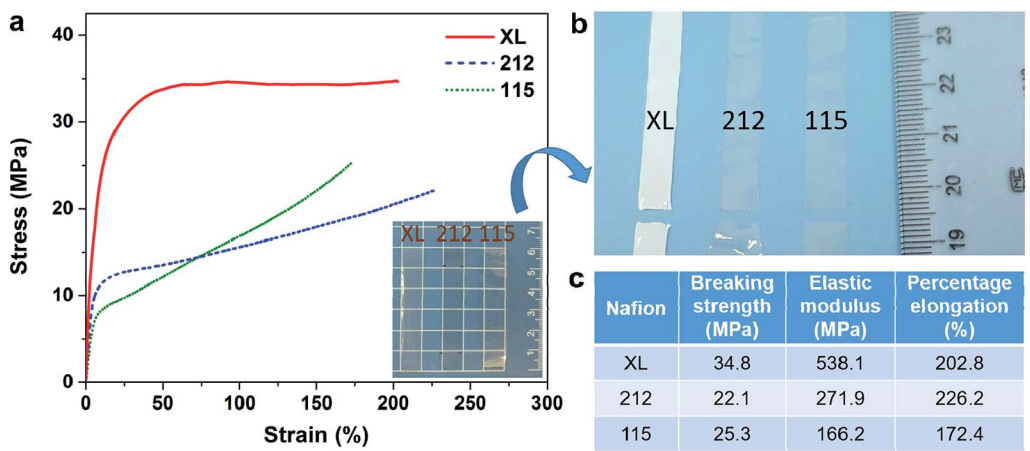

Nafion	Breaking strength (MPa)	Elastic modulus (MPa)	Percentage elongation (%)
XL	34.8	538.1	202.8
212	22.1	271.9	226.2
115	25.3	166.2	172.4

Fig. 2 Mechanical properties of various Nafion membranes: (a) strain–stress curves (inset shows the photograph of the samples before test), (b) photograph of the fracture, and (c) mechanical properties.

Table 2 Physicochemical and transport properties of various Nafion membranes

Nafion	Thickness (dry, μm)	Thickness (wet, μm)	Swelling ratio (though-plane, %)	Swelling ratio (in-plane, %)	Area resistance (Ω cm^2)	VO^{2+} permeability (10^{-7} cm^2 min^{-1})
XL	30	40	33.3	6.0	0.30	1.1
212	52	61	17.3	17.0	0.39	5.7
115	125	150	20.0	18.0	0.52	10.9

suggesting that thinner Nafion membrane is easier to absorb water.[15,42] On the contrary, the in-plane swelling ratio of the XL membrane is much smaller (Fig. S1†) than those of 212 and 115 membranes (6.0% *vs.* 17.0% and 18.0%), due to that the hydrophilic Nafion layer is coated on the hydrophobic microporous PTFE-rich substrate and the microporous substrate would suppress the in-plane size enlargement. The swelling mode that the thickness (ion transport direction) increases while the in-plane size remains stable may be helpful to decrease the crossover of vanadium ions (by extending the transport path), which will be discussed below.

Area resistance is another important parameter of IEM which determines the voltage efficiency (VE) and rate performance of a VFB.[43] Compared with proton conductivity, area resistance can more accurately reflect whether the film is suitable for the VFB application.[7,30] In this work, we use a VFB single cell method to measure the area resistance of the membrane (Fig. S2†),[16] since the contact media has a great impact on the area resistance. Nyquist plots of VFBs based on XL, 212 and 115 membranes are presented in Fig. 3a. They similarly show a high-frequency intercept for the bulk (internal) resistance (R_b) and a low-frequency intercept for the total resistance (R_t). The sum of mass transport resistance and activation resistance (R_p) of the VFB can be achieved by subtracting R_b from R_t, which is mainly determined by the activity of the electrode.[31,44] The resistance of membranes is obtained by subtracting the blank resistance (the single cell without membrane) from R_b, as shown in the inset of Fig. 3a. The calculated area resistance of XL, 212 and 115 membranes is 0.30, 0.39 and 0.52 Ω cm^2, respectively. Although wet pretreatment (merged in deionized water for 24 h) can further decrease the area resistance of XL membrane (Fig. S2†), the curled wet XL membrane (Fig. S1†) is not favorable for large-scale VFB assembly processing. Besides, in aspects of rate performance and cycling stability, the as-received XL membrane performs no worse than the wet one as shown in Fig. S3.† Therefore, the XL membrane is used directly in the following VFB evaluation.

Vanadium ion permeability, mainly influenced by the ionic micelle nanostructure and ion transport mechanism of IEM, is a crucial factor in determining the coulombic efficiency (CE) and capacity fading of VFB.[8,31] VO^{2+} crossover plots through three Nafion membranes were tested by the diffusion cell as shown in Fig. 3b. The obtained VO^{2+} permeability for different membranes is listed in Table 2. Surprisingly, the thinnest XL membrane exhibits the smallest VO^{2+} permeability (1.1×10^{-7} cm^2 min^{-1}), which is an order of magnitude lower than that of 115 membrane (10.9×10^{-7} cm^2 min^{-1}). Although the 212 membrane is much thinner than the 115 membrane (61 μm *vs.* 150 μm, in wet status), the 212 membrane shows only slightly faster VO^{2+} crossover rate than that of the 115 membrane. Actually, the 212 membrane demonstrates slow VO^{2+} permeability compared to the 115 membrane (see Table 2). This may be explained by that the 212 membrane is prepared by solution casting to minimize the number of defects, while the 115 membrane is an extruded membrane.[45] The different fabrication process may cause different microstructure and accordingly the membrane thickness may not correlate linearly with the VO^{2+} permeability. To gain deeper insights into the structure–transport relationship of three membranes, the cross-section SEM images of various membranes are compared in the inset of Fig. 3b. Obviously, the sandwich structure (dense Nafion/microporous PTFE/dense Nafion) of XL membrane would obey different vanadium crossover mechanism with those dense structure 212 and 115 membranes. In our opinion,

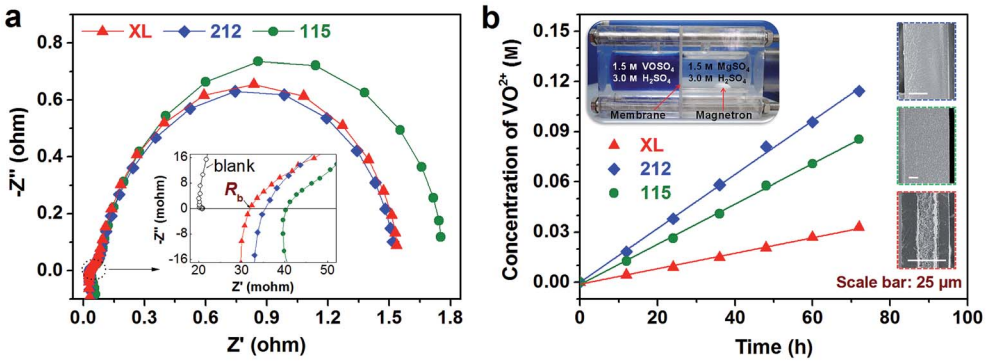

Fig. 3 Ion transport properties of various Nafion membranes: (a) Nyquist plots of VFBs assembled with various membranes, (b) VO^{2+} crossover plots (inset shows the cross-section SEM images of various membranes).

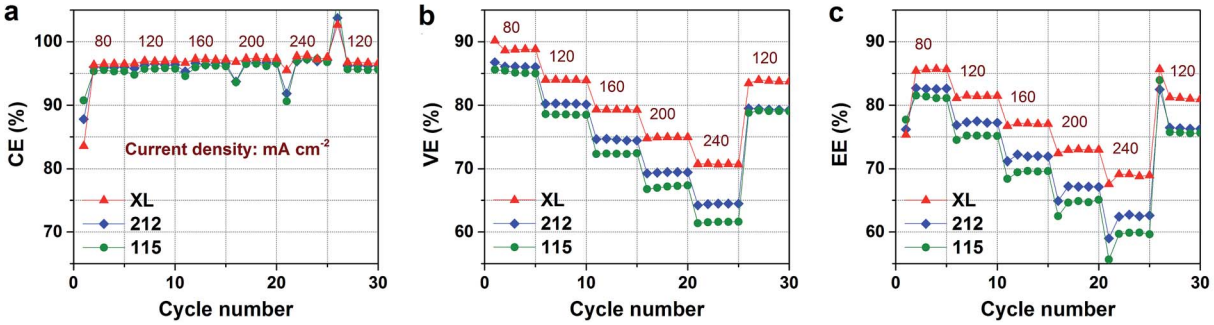

Fig. 4 Rate performances of VFBs assembled with various Nafion membranes: (a) coulombic efficiency, (b) voltage efficiency, (c) energy efficiency.

the extremely lower VO^{2+} permeability of XL membrane may be attributed to its middle hydrophobic microporous PTFE layer, which can effectively suppress the aqueous vanadium electrolyte crossover. It is expected that the smaller area resistance and lower vanadium ion permeability of XL membrane would lead to higher VE and CE of VFB, which will be demonstrated in the subsequent single cell test.

3.2. Excellent rate capability

High-rate capability is beneficial to reduce the cost per unit power of VFB.[5,31,46] Rate performance of VFBs assembled with XL, 212, and 115 membranes is shown in Fig. 4. All VFBs can operate stably under the current density from 40 to 240 mA cm^{-2}. Notably, all the three membranes-based VFBs exhibit the typical trend with the increase of current density: CE increases slightly with current density increasing, while VE and energy efficiency (EE) illustrate the opposite. The CE of a VFB is mainly affected by vanadium ion crossover[7–9] and in all test current densities, the XL membrane shows higher CE than the 212 and 115 membranes confirming the better permeability hindering effect of XL membrane (Fig. 3b). As shown in Fig. 4a, CE value of the 212 membrane is slightly higher than that of the 115 membrane at all current densities. The difference between the VO^{2+} crossover and CE results may be assigned to the combined impact of various vanadium ions (*i.e.* V^{2+}, V^{3+}, VO^{2+} and VO_2^+) crossover during charge–discharge process. In aspects of VE, the internal resistance (R_b) of the VFB would play a dominant role.[31] The XL membrane shows much higher VE than its counterparts in all testing current densities (Fig. 4b), agreeing well with the area resistance results in Fig. 3a. Besides, the gap of VE between XL and 212 (115) increases with the operation current density because of the increased ohmic polarization. Under the mutual effect of CE and VE, the XL membrane demonstrates much higher EE than that of 212 and 115 membranes, as shown in Fig. 4c. It is worth noting that the EE of XL can reach 70% even under the current density of 240 mA cm^{-2}. Moreover, the XL membrane can operate stably at the current density up to 400 mA cm^{-2} (Fig. S3†).

The excellent rate capability of the XL membrane can also observed directly from the charge–discharge curves. Fig. 5a and b illustrate the charge–discharge curves of various membranes under current densities of 120 mA cm^{-2} and 200 mA cm^{-2}, respectively. It is obvious that the XL based VFB presents lower charge curves and higher discharge curves than the 212 and 115 membranes under the both current densities because of the lower area resistance of the XL membrane. A rise of charge voltage and a decline of discharge voltage as well as a reduction in charge–discharge capacity are found with the increased current density, attributed to the increased polarization losses with the increased current density. In addition to efficiency parameters, electrolyte utilization (EU) is another important evaluation index of VFB. High EU is essential to improve the energy density of a VFB. In this work, EU is defined as the ratio of actual discharge capacity to theory capacity. Fig. 5c shows the EU of VFBs at the operating current densities ranging from 80 mA cm^{-2} to 240 mA cm^{-2}. EUs of all VFBs decrease with the

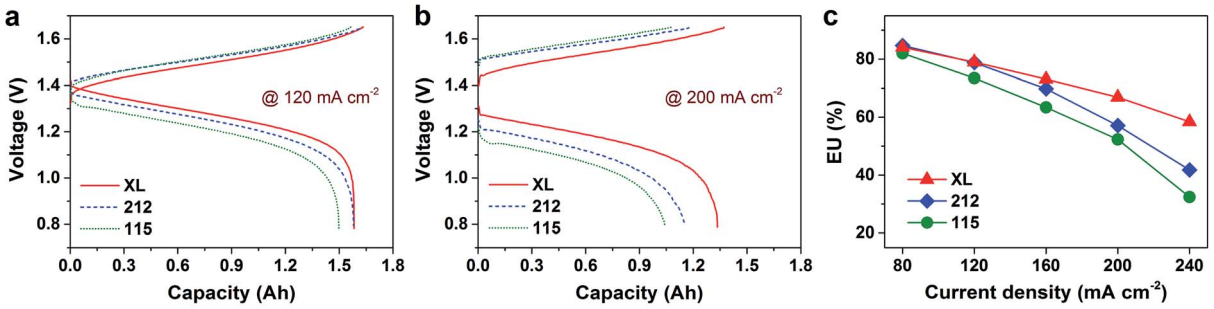

Fig. 5 Charge–discharge curves (a and b) and electrolyte utilization (c) of VFBs assembled with various Nafion membranes.

increasing current density. The VFB based on XL membrane, with lowest area resistance (Fig. 3a) and vanadium ions permeability (Fig. 3b), exhibits lower decline rate than others. This is mainly due to that the increasing current density would cause higher ohmic and electrochemical polarization.

3.3. Outstanding cycling stability

To further investigate the cycling stability of the XL membrane, VFB single cells assembled with various membranes were run continuously at a medium current density of 120 mA cm^{-2} and voltage window of 0.8–1.65 V. All VFBs were started at the same time to eliminate the system error. The ambient temperature was controlled at 25 ± 2 °C during the whole testing process. The cycling performances including CE, EE, and discharge capacity fading are illustrated in Fig. 6. It can be seen that the CE of all Nafion membranes remain nearly stable during the whole cycling test, suggesting that there is no obvious degradation or ionic micelle nanostructure change happening under the VFB operation. The EE of 212 membrane gradually decay for about 5%, while that of XL and 115 membranes keep stable during 500 cycles test. Besides, the EE of XL membrane shows higher value than 212 and 115 membranes during all the cycling test because of its lowest area resistance as shown in Table 2.

Owing to the excellent rate performance, the XL membrane exhibits the highest discharge capacity during lifespan test (Fig. 6b). Electrolyte imbalance and capacity fading in VFB are mainly caused by vanadium ion crossover.[8] Therefore, the 212 membrane shows the fast capacity fading rate because of its highest vanadium ion permeability (Table 2). In contrast, the XL and 115 membranes show comparable capacity retention in each of the 100 cycles (see detail in Fig. 6b). For instance, after 500 cycles, the discharge capacity retention of the XL, 212, and 115 membrane is 56.5%, 45.9%, and 55.2%, respectively. Moreover, four steps can be seen in the capacity change curves of all membranes: (1) capacity increases gradually (cycle nos. 1–4); (2) capacity decays rapidly (cycle nos. 5–45); (3) capacity rebounds slightly or remains stable (cycle nos. 46–80); (4) capacity decays slowly and linearly (after 80 cycles). This uncommon trend may be due to the initial $V^{3.5+}$ electrolyte ($VO^{2+}/V^{3+} = 1/1$) used in this study.[31]

The long-term cycling stability is very essential for the safe operation of VFBs.[5,7] Previous studies have demonstrated that the benchmark 212 and 115 membranes have excellent durability for VFB application.[6,16,31] To further assess the advantages of the sandwich structured XL membrane in the VFB, super long-term cycling test is conducted continuously at a medium current density of 120 mA cm^{-2} with sudden elevating to a high current density of 200 mA cm^{-2} from cycle sequence of 600 to 1600 as shown in Fig. 7. The results are displayed by three test periods, the first from 0 to 600 cycles, the second from 601 to 1600 cycles, the third from 1600 to 2200 cycles. It can be seen that the CE and EE of XL based VFB remain nearly stable during each cycle test period, indicating that there is no obvious nanostructure change during the super long-term cycling even though the current density is changed. The values of CE and EE at 120 and 200 mA cm^{-2} are consistent with the rate performance test in Fig. 4. EIS test is performed at each stage to monitor the resistance change of the membrane. As shown in the inset of Fig. 7, Nyquist plots (high-frequency region) of the initial VFB and the VFB after 600, 1600, and 2200 cycles are nearly overlap (*i.e.* the internal resistance R_b remains stable), demonstrating superior stable ion transport properties of the XL membrane. The outstanding stability of XL membrane can be assigned to the unique sandwich structure (Fig. 1), in which the middle microporous PTFE reinforcement layer plays a very important role.

3.4. All-climate operation

The wide temperature adaptability of VFB is a critical issue which affect its safety application. In the real world application, VFB unavoidably faces a variety of harsh climatic conditions (extremely cold or hot). Therefore, investigating VFB under the all-climate range is very essential to its practical application around the whole globe.[30,41,47,48] Fig. 8a depicts the homemade

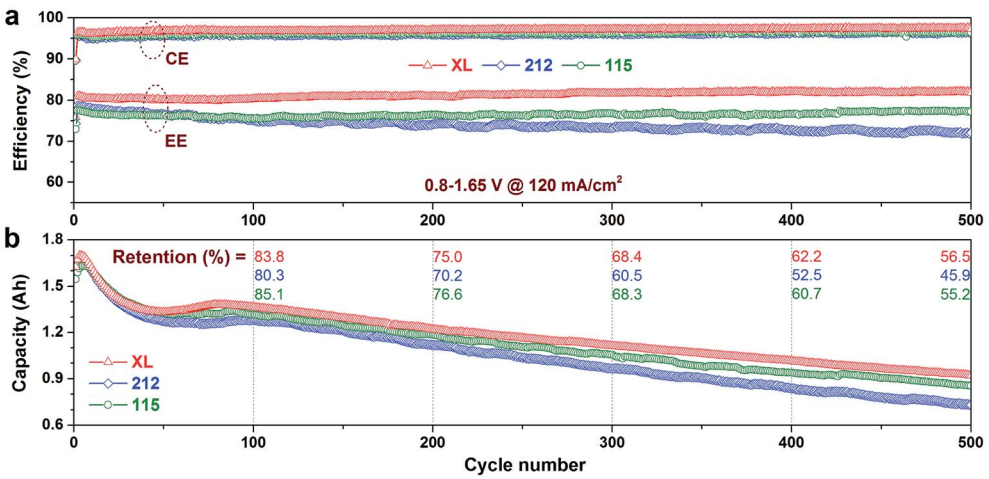

Fig. 6 Cycling performances of VFBs assembled with various Nafion membranes at current density of 120 mA cm^{-2}: (a) coulombic efficiency and energy efficiency, (b) discharge capacity and capacity retention.

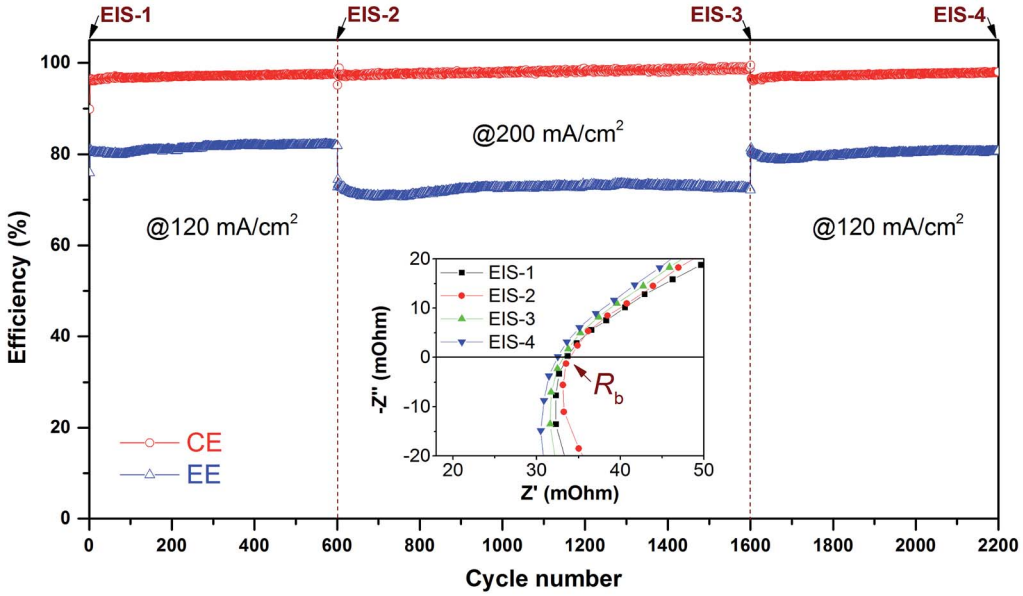

Fig. 7 Super long-term cycling stability of VFBs assembled with Nafion XL membrane. Inset shows the Nyquist plots of the initial VFB (EIS-1) and the VFB after 600 (EIS-2), 1600 (EIS-3), and 2200 (EIS-4) cycles.

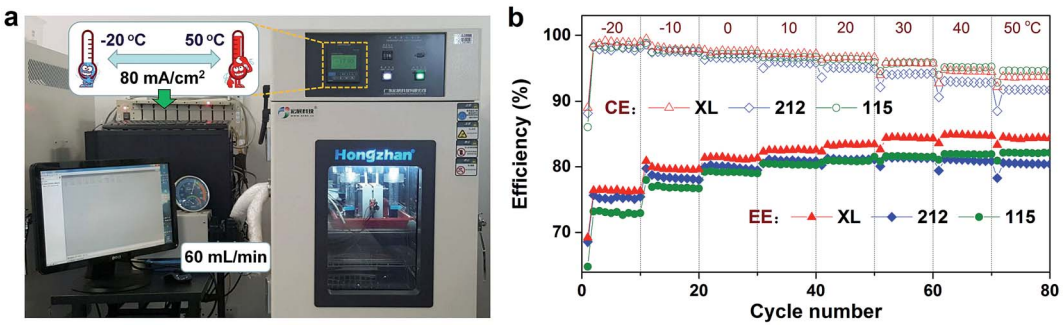

Fig. 8 All-climate performances of VFBs assembled with various Nafion membranes at current density of 80 mA cm^{-2}: (a) photograph of the test platform, (b) coulombic efficiency and energy efficiency as a function of temperature.

all-climate research platform of VFB. VFB single cell and the electrolyte tanks were put in the thermostat and driven by an outside peristaltic pump. All the pipes were prevented from temperature fluctuation. The VFB was ran for 10 cycles at each temperature point from −20 °C to 50 °C under current density of 80 mA cm^{-2}. Performances under this all-climate test of VFBs based on the three membranes are illustrated in Fig. 8b. All the three membranes based VFBs run stably during the whole temperature range, but their CE decreases gradually because of the accelerated vanadium ion crossover with the temperature increasing from −20 °C to 50 °C.[49,50] As the temperature increases, the CE of the 212 membrane decreases faster, due to the fact that the very thin 212 membrane is easy to swollen at high temperatures. On the contrary, because of the reinforcement of the middle microporous PTFE layer, the XL membrane may still maintain a good nanostructure stability at high temperatures.[35] In contrast to CE, the VE of all VFBs increases with temperature because of the decreased polarization resistance (*i.e.* enhanced electrochemical activity of electrodes) and ohmic resistance (*i.e.* improved transport properties). Since the EE of a VFB is determined by the mutual effect of CE and VE, the XL membrane shows the highest EE through the whole temperature range as shown in Fig. 8b, which confirms the feasibility of its application in VFB for all-climate energy storage.

4. Conclusions

In summary, a novel sandwich structure membrane, Nafion XL, consisting of a microporous PTFE middle layer (around 10 μm) and two dense Nafion outer layers (around 10 μm), is evaluated towards VFB application and compared with the widely used Nafion 212 and 115 membranes. The ultra-thin sandwich structure can combine the advantages of microporous PTFE (effective mechanical reinforcement) and dense Nafion membrane (fast proton transport), offering excellent performances in VFB. In terms of physicochemical properties, the XL membrane owns lower area resistance and VO^{2+} permeability

than the 115 and 212 membranes. Therefore, the XL membrane demonstrates higher CE, VE and EE as well as electrolyte utilization than the 212 and 115 membranes under the current density from 40 to 240 mA cm^{-2}. Moreover, the XL membrane can operate stably at the current density up to 400 mA cm^{-2}. Thanks to the reinforcement effect of microporous PTFE layer, the XL membrane exhibits very stable efficiencies (97% of CE and 81% of EE) and slower capacity fading rate (0.087% per cycle) during 500 cycle's charging–discharging test at current density of 120 mA cm^{-2}. In addition, the XL membrane can maintain nanostructure stability during wide temperature test, and shows higher EE than the 212 and 115 membranes through the temperature range from −20 °C to 50 °C. More importantly, because the cost of microporous PTFE is significantly lower and the dense Nafion layer is very thin (only 20 μm), the XL membrane will promise much lower cost than the 212 (50 μm) and 115 (125 μm) membranes. The excellent rate performance, outstanding cycling stability, all-climate adaptability and relatively low-cost indicating that the Nafion XL membrane can successfully replace the more expensive Nafion series membranes for using in VFB.

Acknowledgements

This work was supported by the Basic Research Project of Shenzhen City (Nos. JCYJ20150630114140630 and JCYJ20170307152754218) and the Natural Science Foundation of Guangdong Province (Nos. 2016A030310025 and 2015A030313894). The authors would like to thank Mr Yang Zhao for mechanism property testing.

References

1 Z. Yang, J. Zhang, M. C. Kintner-Meyer, X. Lu, D. Choi, J. P. Lemmon and J. Liu, *Chem. Rev.*, 2011, **111**, 3577.
2 M. Ulaganathan, V. Aravindan, Q. Yan, S. Madhavi, M. Skyllas-Kazacos and T. M. Lim, *Adv. Mater. Interfaces*, 2016, **3**, 1500309.
3 A. Parasuraman, T. M. Lim, C. Menictas and M. Skyllas-Kazacos, *Electrochim. Acta*, 2013, **101**, 27.
4 P. Leung, X. Li, C. P. De León, L. Berlouis, C. J. Low and F. C. Walsh, *RSC Adv.*, 2012, **2**, 10125.
5 M. Park, J. Ryu, W. Wang and J. Cho, *Nat. Rev. Mater.*, 2017, **2**, 16080.
6 C. Ding, H. Zhang, X. Li, T. Liu and F. Xing, *J. Phys. Chem. Lett.*, 2013, **4**, 1281.
7 X. Li, H. Zhang, Z. Mai, H. Zhang and I. Vankelecom, *Energy Environ. Sci.*, 2011, **4**, 1147.
8 B. Schwenzer, J. Zhang, S. Kim, L. Li, J. Liu and Z. Yang, *ChemSusChem*, 2011, **4**, 1388.
9 T. K. Hoang and P. Chen, *RSC Adv.*, 2015, **5**, 72805.
10 K. A. Mauritz and R. B. Moore, *Chem. Rev.*, 2004, **104**, 4535.
11 A. Kusoglu and A. Z. Weber, *Chem. Rev.*, 2017, **117**, 987.
12 J. Xi, Z. Wu, X. Qiu and L. Chen, *J. Power Sources*, 2007, **166**, 531.
13 L. Yu, F. Lin, L. Xu and J. Xi, *RSC Adv.*, 2016, **6**, 3756.
14 D. Reed, E. Thomsen, W. Wang, Z. Nie, B. Li, X. Wei, B. Koeppel and V. Sprenkle, *J. Power Sources*, 2015, **285**, 425.
15 B. Jiang, L. Wu, L. Yu, X. Qiu and J. Xi, *J. Membr. Sci.*, 2016, **510**, 18.
16 Y. Zhou, L. Yu, J. Wang, L. Liu, F. Liang and J. Xi, *RSC Adv.*, 2017, **7**, 19425.
17 C. Minke and T. Turek, *J. Power Sources*, 2015, **286**, 247.
18 R. V. Noorden, *Nature*, 2014, **507**, 26.
19 D. W. Shin, M. D. Guiver and Y. M. Lee, *Chem. Rev.*, 2017, **117**, 4759.
20 J. Xi, Z. Li, L. Yu, B. Yin, L. Wang, L. Liu, X. Qiu and L. Chen, *J. Power Sources*, 2015, **285**, 195.
21 Y. Zhang, S. Zhang, X. Huang, Y. Zhou, Y. Pu and H. Zhang, *Electrochim. Acta*, 2016, **210**, 308.
22 C. Wu, S. Lu, H. Wang, X. Xu, S. Peng, Q. Tan and Y. Xiang, *J. Mater. Chem. A*, 2016, **4**, 1174.
23 J. K. Jang, T. H. Kim, S. J. Yoon, J. Y. Lee, J. C. Lee and Y. T. Hong, *J. Mater. Chem. A*, 2016, **4**, 14342.
24 B. Yin, Z. Li, W. Dai, L. Wang, L. Yu and J. Xi, *J. Power Sources*, 2015, **285**, 109.
25 T. Mohammadi and M. Skyllas-Kazacos, *J. Appl. Electrochem.*, 1997, **27**, 153.
26 W. Dai, L. Yu, Z. Li, J. Yan, L. Liu, J. Xi and X. Qiu, *Electrochim. Acta*, 2014, **132**, 200.
27 Z. Yuan, X. Li, J. Hu, W. Xu, J. Cao and H. Zhang, *Phys. Chem. Chem. Phys.*, 2014, **16**, 19841.
28 L. Yu and J. Xi, *ACS Appl. Mater. Interfaces*, 2016, **8**, 23425.
29 S. Kim, T. B. Tighe, B. Schwenzer, J. Yan, J. Zhang, J. Liu, Z. Yang and M. A. Hickner, *J. Appl. Electrochem.*, 2011, **41**, 1201.
30 J. Xi, B. Jiang, L. Yu and L. Liu, *J. Membr. Sci.*, 2017, **522**, 45.
31 B. Jiang, L. Yu, L. Wu, D. Mu, L. Liu, J. Xi and X. Qiu, *ACS Appl. Mater. Interfaces*, 2016, **8**, 12228.
32 G. M. Geise, M. A. Hickner and B. E. Logan, *ACS Appl. Mater. Interfaces*, 2013, **5**, 10294.
33 DuPont, Product Information: Nafion XL PFSA Membrane, 2010.
34 https://www.chemours.com/Nafion/en_US/products/nafion.html.
35 S. Shi, A. Z. Weber and A. Kusoglu, *J. Membr. Sci.*, 2016, **516**, 123.
36 M. P. Rodgers, L. J. Bonville, R. Mukundan, R. L. Borup, R. Ahluwalia, P. Beattie, R. P. Brooker, N. Mohajeri, H. R. Kunz, D. K. Slattery and J. M. Fenton, *ECS Trans.*, 2013, **58**, 129.
37 Z. Li, W. Dai, L. Yu, J. Xi, X. Qiu and L. Chen, *J. Power Sources*, 2014, **257**, 221.
38 Z. Li, W. Dai, L. Yu, L. Liu, J. Xi, X. Qiu and L. Chen, *ACS Appl. Mater. Interfaces*, 2014, **6**, 18885.
39 W. Dai, Y. Shen, Z. Li, L. Yu, J. Xi and X. Qiu, *J. Mater. Chem. A*, 2014, **2**, 12423.
40 L. Wu, J. Wang, Y. Shen, L. Liu and J. Xi, *Phys. Chem. Chem. Phys.*, 2017, **19**, 14708.
41 S. Xiao, L. Yu, L. Wu, L. Liu, X. Qiu and J. Xi, *Electrochim. Acta*, 2016, **187**, 525.
42 W. Xie, R. M. Darling and M. L. Perry, *J. Electrochem. Soc.*, 2016, **163**, A5084.

43 X. Wu, J. Hu, J. Liu, Q. Zhou, W. Zhou, H. Li and Y. Wu, *Pure Appl. Chem.*, 2014, **86**, 633.
44 L. Wu, Y. Shen, L. Yu, J. Xi and X. Qiu, *Nano Energy*, 2016, **28**, 19.
45 S. Naudy, F. Collette, F. Thominette, G. Gebel and E. Espuche, *J. Membr. Sci.*, 2014, **451**, 293.
46 K. J. Kim, M. S. Park, Y. J. Kim, J. H. Kim, S. X. Dou and M. Skyllas-Kazacos, *J. Mater. Chem. A*, 2015, **3**, 16913.
47 J. Xi, S. Xiao, L. Yu, L. Wu, L. Liu and X. Qiu, *Electrochim. Acta*, 2016, **191**, 695.
48 C. Choi, S. Kim, R. Kim, Y. Choi, S. Kim, H. Jung, J. H. Yang and H. Kim, *Renewable Sustainable Energy Rev.*, 2017, **69**, 263.
49 X. Wei, Z. Nie, Q. Luo, B. Li, B. Chen, K. Simmons, V. Sprenkle and W. Wang, *Adv. Energy Mater.*, 2013, **3**, 1215.
50 D. Mu, L. Yu, L. Liu and J. Xi, *ACS Sustainable Chem. Eng.*, 2017, **5**, 2437.